Towards numerical simulation of wave impacts in an LNG tank

Ronald A. Remmerswaal and Arthur E.P. Veldman[*]

Bernoulli Institute, University of Groningen, The Netherlands

[*] Corresponding author: `a.e.p.veldman@rug.nl`

1 Introduction

During the transport of Liquefied Natural Gas (LNG) in LNG carriers sloshing can dangerously interfere with the ship motion through violent breaking-wave impacts with the container walls. The role of free surface instabilities during these impacts is not well understood [Lafeber et al., 2012]; we will study it via computer simulation. Its numerical modeling involves dealing with multi-phase flow, featuring a multitude of jumps (discontinuities) of fluid properties across the interface separating the fluids. The thin shear layers around the interface usually are numerically underresolved and result in unphysical interaction between the two fluids. Such an underresolved layer is numerically better described by a velocity field which has a (contact) discontinuity in the tangential direction.

2 Mathematical model

The equations for *incompressible Euler flow* describe the conservation of mass and momentum in each of the phases $\pi = l, g$ (liquid and gas) in an arbitrary control volume $\omega = \omega^l \cup \omega^g$

$$\frac{\mathrm{d}}{\mathrm{d}t} \int_{\omega^\pi} \rho^\pi \, \mathrm{d}V + \int_{\partial\omega^\pi \setminus I} \rho^\pi u_\eta^\pi \, \mathrm{d}S = 0 \tag{1}$$

$$\frac{\mathrm{d}}{\mathrm{d}t} \int_{\omega^\pi} \rho^\pi \mathbf{u}^\pi \, \mathrm{d}V + \int_{\partial\omega^\pi \setminus I} \rho^\pi \mathbf{u}^\pi u_\eta^\pi \, \mathrm{d}S = - \int_{\partial\omega^\pi} (p^\pi - \rho^\pi \mathbf{g} \cdot \mathbf{x})\boldsymbol{\eta} \, \mathrm{d}S, \tag{2}$$

where $\boldsymbol{\eta}$ denotes the face normal, u_η^π the face normal velocity component, p^π the pressure, $\mathbf{g}$ the gravitational acceleration and ρ^π the density per phase. We consider incompressible flow for which the mass conservation equations result in a volume constraint on the evolution of the interface

$$\frac{\mathrm{d}}{\mathrm{d}t} |\omega^l| + \int_{\partial\omega^l \setminus I} u_\eta^l \, \mathrm{d}S = 0, \quad \text{where } |\omega^\pi| \text{ denotes the volume of } \omega^\pi. \tag{3}$$

The influence of surface tension, relevant in this application, is included via Laplace's law

$$[\![p]\!] := p^g - p^l = -\sigma\kappa. \tag{4}$$

Here κ denotes the interface mean curvature and $[\![p]\!]$ denotes the jump of p over the free surface. We assume immiscible fluids without phase change, and therefore $[\![u_\eta]\!] = \boldsymbol{\eta} \cdot (\mathbf{u}^g - \mathbf{u}^l) = 0$. Together with appropriate boundary conditions on $\mathbf{u}^\pi$ and a contact angle boundary condition on κ, this results in a closed system of equations. Note that this model does not impose any smoothness on the tangential velocity component $u_\tau = \boldsymbol{\tau} \cdot \mathbf{u}$, where $\boldsymbol{\tau}$ denotes the interface tangent.

Addition of the mass conservation equations, when divided by their respective densities, yields

$$\int_{\partial\omega} u_\eta \, \mathrm{d}S = \int_{\partial\omega^l \setminus I} u_\eta^l \, \mathrm{d}S + \int_{\partial\omega^g \setminus I} u_\eta^g \, \mathrm{d}S = 0, \tag{5}$$

thus showing that the mixture velocity field is divergence free. Taking the time derivative of the divergence constraint, substituting the momentum equation and using $[\![u_\eta]\!] = 0$, yields

$$\int_{\partial\omega} \frac{1}{\rho} \, \partial_\eta p \, \mathrm{d}S = - \int_{\partial\omega} \boldsymbol{\eta} \cdot (\mathbf{u} \cdot \nabla)\mathbf{u} \, \mathrm{d}S. \tag{6}$$

We supplement the aforementioned equation with Laplace's law (4), a homogeneous Neumann boundary condition on the pressure along the side walls, and a jump condition on the normal pressure gradient at the interface which is necessary for well-posedness:

$$\left[\!\left[\frac{1}{\rho} \, \partial_\eta p \right]\!\right] = - \left[\!\left[\boldsymbol{\eta} \cdot \frac{D\mathbf{u}}{Dt} \right]\!\right]. \tag{7}$$

It follows directly from the strong form of the Euler equations.

3   Numerical model

Notation The cells in the staggered rectilinear (Arakawa C) grid constitute the set C, with faces $\mathcal{F}(c)$ for $c \in C$. A time-dependent subset $\mathcal{F}_I$ of the faces is cut by the interface $I(t) \subset \Omega$; these are split into their liquid and gaseous parts: $f = f^g \cup f^l$. This defines the set $\hat{\mathcal{F}}^\pi$ of all the (possibly cut) faces which are entirely contained in the π-phase; let $\hat{\mathcal{F}} = \hat{\mathcal{F}}^l \cup \hat{\mathcal{F}}^g$(Fig. 1a). The functions defined on C form C^h, with e.g. $p \in C^h : c \mapsto p_c \approx p(\mathbf{x}_c)$, where $\mathbf{x}_c$ is the center of cell c. Similarly, we have the space F^h defined in the center $\mathbf{x}_f$ of the face f with normal $\boldsymbol{\eta}_f$, whereas $\alpha : C \times \mathcal{F} \to \{1, -1\}$ encodes the orientation of the face normals, with $\alpha_{c,f}\boldsymbol{\eta}_f$ pointing outward.

3.1   Momentum equations

In the interior of each of the phases, the momentum equations are discretized using the symmetry-preserving finite-volume method of [Verstappen and Veldman, 2003]. Near the interface we choose to discretize the momentum equations in strong form, thereby sacrificing exact momentum conservation but alleviating difficulties faced with arbitrarily small cells $|c^\pi|(t)$ and non-smooth-in-time face areas $|f^\pi|(t)$. At the interface we use a first-order upwind convection scheme *per phase*, which relies on linear extrapolation of velocities. The interface is represented using the volume fraction field $\bar{\chi} = |c^l|/|c| \in C^h$ as per the Volume-of-Fluid method. Advection of the interface is performed using the Lagrangian-Eulerian Advection Scheme (LEAS) [Zinjala and Banerjee, 2015].

The time integration is performed under a CFL constraint of 0.5 using a second-order accurate explicit method, followed by a pressure correction step

$$\frac{u_f^* - u_f^{(n)}}{\Delta t} = R\left(\frac{3}{2}u_f^{(n)} - \frac{1}{2}u_f^{(n-1)}\right)_f, \quad u_f^{(n+1)} = u_f^* - \frac{\Delta t}{\rho}(Gp)_f, \quad \forall f \in \hat{\mathcal{F}}. \tag{8}$$

Here R denotes the convection and gravity terms, and $G : C^h \to \hat{F}^h$ is the gradient operator.

The pressure implicitly couples the two phases. To make the velocity field divergence free, the Laplace operator is decomposed in a divergence $\bar{D} : \hat{F}^h \to C^h$ and a gradient G:

$$\bar{D}\left(\frac{1}{\rho}Gp\right)_c = \bar{D}(u^*)_c, \quad \forall c \in C. \tag{9}$$

The gradient G contains the value jump due to capillarity, as well as the jump in the normal derivative.

At the interface the velocity field is discontinuous, and the divergence operator needs to be modified. A finite-difference Ghost Fluid Method (GFM) [Liu et al., 2000] will result in an incompatible discretization of the pressure Poisson problem. As there will be functions $u \in \hat{F}_0^h$, i.e. vanishing at the boundary, which are not solenoidal, hence do not all satisfy a discrete Gauss divergence theorem. A consequence of this incompatibility is that the resulting pressure Poisson equation has no solution.

A finite-volume approach naturally preserves the flux cancellation property which a divergence operator should satisfy, and hence all solutions in $\hat{F}_0^h$ do satisfy a discrete Gauss theorem. We choose the cut-cell method [Udaykumar et al., 1997]. Face apertures $A_f \in F^h$ are computed (from the PLIC reconstruction) as the fraction of the face $f \in \mathcal{F}$ contained in the reference fluid l, so $A_f = |f^l|/|f|$. This gives the divergence operator

$$|c|\bar{D}(u)_c = \sum_{f \in \mathcal{F}(c)} \alpha_{c,f}|f|\bar{u}_f, \tag{10}$$

where we define the mixture velocity $\bar{u}_f = A^f u_f^l + (1 - A^f)u_f^g$ (Fig. 1a).

In the interior of the phases we define the gradient G as a standard finite difference operator. Near the interface the gradient needs modification to sharply capture the imposed jumps, as will be described next.

3.2   The Ghost Fluid Method

We consider a finite-difference approximation for the gradient at a face $f \in \mathcal{F}_I$ near the interface. The pressure $p \in C^h$ is defined point-wise according to the liquid indicator $\chi \in C^h$ ($\chi = 1$ in liquid and $\chi = 0$ in gas). Now, consider a face f which connects two nodes $C(f) = \{c, c'\}$ from different phases

(a) CCM: Each face is split into its liquid and gaseous part $f = f^l \cup f^g$. Shaded region corresponds to the liquid parts c^l, c'^l.

(b) GFM: The pressure values denoted by $\tilde{p}$ are 'ghost' pressures and not actually part of the solution.
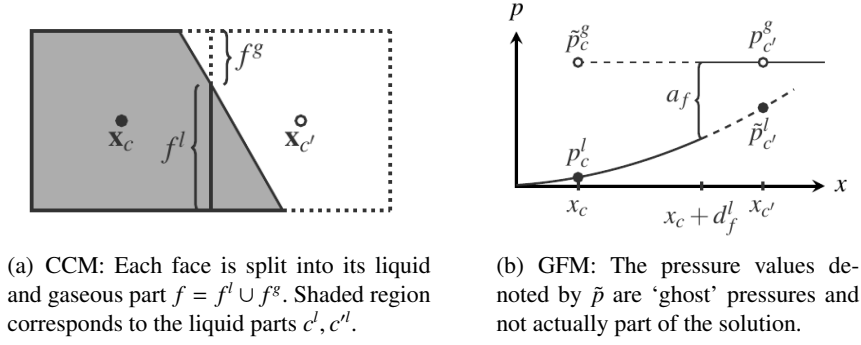
Fig. 1: Illustration of the cut-cell method (CCM: left) and the ghost fluid method (GFM: right).

(so $\chi_c \neq \chi_{c'}$). Hence we know the liquid pressure p_c^l on one side of the face and the gas pressure $p_{c'}^g$ on the other side of the face. Also, we can evaluate the value jump $a_f = -\sigma\kappa_f$ (with κ calculated via a generalized local height function [Popinet, 2009]) and gradient jump b_f. The unkown scaled gradients are denoted by g_f^π (Fig. 1b).

The scaled mixture gradients, as per the Ghost Fluid Method [Liu et al., 2000], are then given by

$$\bar{g}_f = \frac{1}{\bar{\rho}_f}(\bar{G}p)_f = \frac{1}{\bar{\rho}_f}(Gp)_f + \frac{\delta_f a_f}{\bar{\rho}_f h_f} - b_f \frac{\hat{\rho}_f}{\bar{\rho}_f}, \tag{11}$$

where $\bar{\rho}_f$, $\hat{\rho}_f$ are average densities depending on the face aperture A_f and the distance to the interface. The difference between the liquid indicators at opposite sides of the face f is denoted by $\delta_f = h_f(G\chi)_f \in \{-1, 0, 1\}$. If the value jump a_f is known at second order accuracy, it follows that the resulting gradient will be at most first order accurate in h_f.

The jump in the pressure gradient occurs only in the component normal to the interface. In [Liu et al., 2000] it is assumed that the jump component tangential to the interface vanishes: $b_f = \alpha_{i_f,f}[\![u_\eta^*]\!]$, where $\alpha_{i_f,f} = \eta_{i_f} \cdot \eta_f$ is the face normal component of the interface normal η_{i_f}. We refer to this approach as the *'one-dimensional' GFM (1d-GFM)*.

Whenever the interface is not aligned with the face f (hence $|\alpha_{i_f,f}| \neq 1$), the 1d-GFM is inconsistent. A *multi-dimensional GFM (Md-GFM)* has been developed, in which we replace the expression for b_f by a formula which consistently imposes the normal derivative jump condition on the gradient (7). As (7) involves the dot product of the full gradient with the interface normal, for the interpolation to the face f of interface tangential pressure derivatives will be required. The interface configuration, defined by the indicator χ as well as the face apertures $A \in F^h$, defines two types of interface faces where the gradient will be modified:

 - If a face f connects two nodes $C(f) = \{c, c'\}$ from different phases (so $\chi_c \neq \chi_{c'}$) we call this an interface normal face $\in \mathcal{F}_{I_\eta}$ (Fig. 2a).
 - On the other hand, if a face f connects two nodes from the same phase, but with a nontrivial aperture (so $A_f \notin \{0, 1\}$) then we call this an interface tangential face $\in \mathcal{F}_{I_\tau}$ (Fig. 2b).

For the discretization of the gradient operator for an interface normal face we choose two faces $\hat{f}^g \in \hat{\mathcal{F}}^g$, $\hat{f}^l \in \hat{\mathcal{F}}^l$ whose face normals are orthogonal to η_f. From here we define the jump interpolant as (Fig. 2a)

$$(Ju)_f = \eta_f[\![u_f]\!] + \eta_{\hat{f}^g}u_{\hat{f}^g}^g - \eta_{\hat{f}^l}u_{\hat{f}^l}^l, \tag{12}$$

Using this jump interpolant we can consistently impose (7)

$$\eta_{i_f} \cdot \left[(Jg)_f - (Ju^*)_f\right] = 0. \tag{13}$$

Combining (12) and (13), and solving for $[\![g_f]\!]$, yields the jump across the face f

$$b_f^\eta = \frac{\eta_{i_f} \cdot (Ju^*)_f}{\alpha_{i_f,f}} - \frac{\alpha_{i_f,\hat{f}^g}}{\alpha_{i_f,f}}g_{\hat{f}^g}^g + \frac{\alpha_{i_f,\hat{f}^l}}{\alpha_{i_f,f}}g_{\hat{f}^l}^l. \tag{14}$$

(a) Interface normal face $f \in \mathcal{F}_{I_\eta}$.   (b) Interface tangential face $f \in \mathcal{F}_{I_\tau}$.
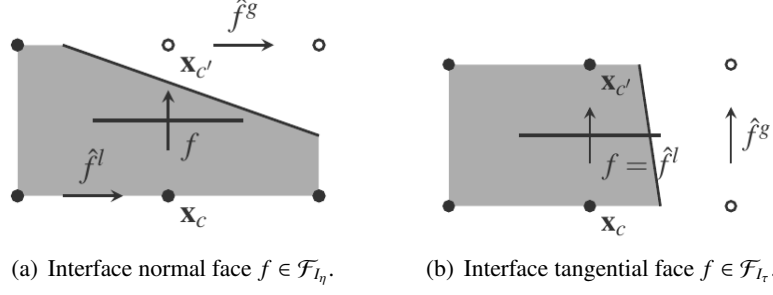
Fig. 2: Examples of Md-GFM gradient stencils.

The faces $\hat{f}^g$, $\hat{f}^l$ should be chosen such that the evaluation of the interpolant can be done explicitly, hence $\hat{f}^\pi \notin \hat{\mathcal{F}}_{I_\eta}$. Moreover, the interpolant should result in a compact 6-point stencil for the Md-GFM gradient. Ensuring $|\alpha_{i_f,\hat{f}^\pi}/\alpha_{i_f,f}| \leq 1$ greatly improves the quality of the Md-GFM operator. For faces $f \in \mathcal{F}_{I_\eta}$ for which this ratio exceeds 1 we interpret the face as an interface tangential face instead.

For an interface tangential face $f \in \mathcal{F}_{I_\tau}$ we select two faces $\hat{f}^g$, $\hat{f}^l$ (one of which coincides with f itself) with the same face normal direction but each in a different phase to be used for computing the gradient jump (Fig. 2b). This results in the following gradient jump

$$b_f^\tau = \frac{1}{\rho^g}(Gp)_{\hat{f}^g} - \frac{1}{\rho^l}(Gp)_{\hat{f}^l}. \tag{15}$$

Composition of the CCM divergence operator with the aforementioned modified gradient operator defines our Laplace operator, with a stencil fitting in 3×3. It is no longer self-adjoint but can still be shown to be negative semi-definite with only the constant pressure in the null-space.

4 Verification and validation

4.1 Poisson problem

We first compare our proposed method to the Immersed Interface Method (IIM) [Leveque and Li, 1994] which sharply imposes jump conditions directly on the Laplacian. Hereto, we consider 'Problem 3' as given by [Leveque and Li, 1994] (with $\beta = \rho^{-1}$):

$$\nabla \cdot \left(\frac{1}{\rho}\nabla p\right) = f, \quad \mathbf{x} \in \Omega = (-1, 1)^2. \tag{16}$$

The right-hand side f, the Dirichlet conditions, as well as the jump conditions at the interface correspond with the exact solution $p = \exp(x)\cos(y)$ when $\mathbf{x} \in \Omega^l$, whereas $p = 0$ when $\mathbf{x} \in \Omega^g$. Here Ω^l is the interior of a circle with radius $\frac{1}{2}$ centered at the origin. Note that p is discontinuous and has a jump in the normal as well as tangential derivative.

N	IIM	1d-GFM	Md-GFM	ρ^g/ρ^l	$\|\frac{1}{\rho}\nabla p - \frac{1}{\rho}Gp^h\|_{L^\infty}$
20	4.38×10^{-4}	7.78×10^{-3}	2.67×10^{-3}	10^6	3.14×10^{-2}
40	1.08×10^{-4}	6.48×10^{-3}	6.15×10^{-4}	10^3	3.14×10^{-2}
80	2.78×10^{-5}	6.47×10^{-3}	1.56×10^{-4}	10^0	3.24×10^{-2}
160	7.50×10^{-6}	3.20×10^{-3}	3.36×10^{-5}	10^{-3}	2.14×10^{-2}
320	1.74×10^{-6}	1.49×10^{-3}	9.11×10^{-6}	10^{-6}	2.14×10^{-2}

Table 1: *(Left)* The error $\|p - p^h\|_{L^\infty}$ for the Poisson problem defined by (16) (IIM results from [Leveque and Li, 1994]). *(Right)* Dependence of the scaled gradient error on the density ratio ρ for the Md-GFM.

We first let $\rho^l = \rho^g = 1$ and vary the mesh-width as $h = 2/N$ where $N = 10 \times 2^l$ for $l = 1, \dots, 5$. The resulting L^∞ errors in the pressure are shown in Table 1a. As expected, the 1d-GFM is first-order accurate, whereas the Md-GFM is second-order accurate, and of comparable accuracy to the IIM. The main advantage of using the Md-GFM is that the Laplace operator itself follows from the *composition* of

a divergence operator and a gradient operator which is required in the context of solving incompressible two-phase problems.

To asses the dependence of the errors on the density ratio we fix the mesh-width $h = 2/80$, and vary the density ratio. The resulting gradient errors are shown in Table 1b. We note that the accuracy of the gradient is independent of the density ratio. Hence the proposed method can be used to accurately simulate near the one-phase limit $\rho^g \to 0$.

4.2 A dambreak problem

The proposed discretization has been implemented in our in-house two-phase Navier-Stokes solver Com-FLOW [Wemmenhove et al., 2015]. Local, adaptive mesh refinement is used, as in [Van der Plas, 2017].

A dambreak problem is studied in a rectangle of size $20 \times 12m$ with an elliptic bathymetry of half lengths 18 and $2.8\,m$ whose center lies in the left-hand side bottom corner. Slip boundary conditions are imposed. The liquid density is given by $\rho^l = 10^3\,kg/m^3$, the gas density varies and will always be indicated. Both fluids are initially at rest and separated by the interface profile $y(x) = 7.6 + 3.6\tanh(0.36(x - 12.5))$. This will result in a flip-through impact (FTI) [Etienne et al., 2018] in which the wave trough and crest reach the wall at the same time instance, resulting in a violent impact. The gravitational acceleration is $g = -9.81\,m/s^2$ and the surface tension $\sigma = 0.072\,J/m^2$ with static contact angle of $90°$.

Our base mesh is uniform with $N_x = 80$ and $N_y = 48$ cells in the x- and y-direction respectively. We consider several levels of mesh refinement, where we refine the mesh near the interface using blocks of size 16×16. The refinement level at the interface $l \in \{2, 3, 4\}$ will always be indicated, the resulting interface mesh-width is given by $h = 2^{-(l+2)}m$.

(a) Standard two-phase model.   (b) Proposed two-phase model.
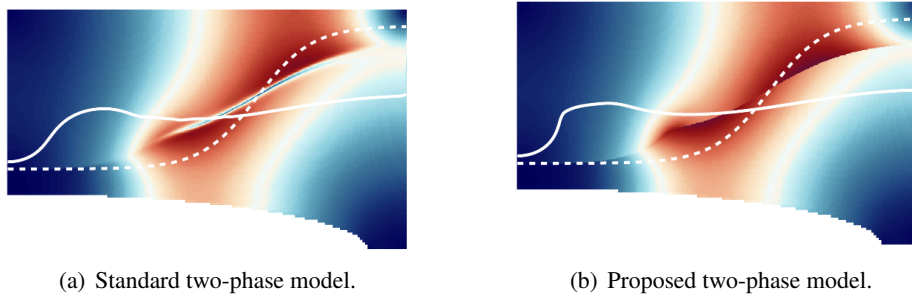
Fig. 3: The absolute velocity $|\mathbf{u}|$ at $t = 0.75$. The interface is shown at $t = 0$ and $t = 1.47$.

We first demonstrate the efficacy of the proposed model when compared to the standard two-phase model for $\rho^g = 1$ and $l = 3$. For this case, Fig. 3 shows the resulting absolute velocity as the initial interface profile (dashed) and at a later time $t = 1.47$ (solid). Note that the standard two-phase model has a thin region at the interface in which the velocity transitions from gas to liquid. Our proposed model captures this transition in a discontinuity, which allows the breaking wave to develop properly, as seen by the interface profile at $t = 1.47$.

To show the dependence of the solution on the gas density, we vary it as $\rho^g = 10^{-3}$, 1, 3 and $5\,kg/m^3$. For the latter three cases a reference exists by CADYF [Etienne et al., 2018]. Figure 4(top) shows a fair agreement in terms of the interface profile. The maximum tangential velocity jump increases as the gas density decreases, which may be expected (Fig. 4(bottom)). For larger gas densities, oscillations in the tangential velocity jump can be observed just before impact, suggesting that free surface instabilities are about to develop. Such oscillations are not present for $\rho^g = 10^{-3}$, meaning that we successfully approach the one-phase limit in which no free surface instabilities due to shearing gas flow are present.

5 Conclusion

We presented a discretization approach for capturing contact discontinuities in two-phase flow, with emphasis on the discretization of the pressure Poisson problem. It imposes smoothness of the velocity field *only in the interface normal direction*. A novel combination of our proposed Md-GFM and the CCM

Fig. 4: Interface profiles (top) and velocity discontinuity (bottom) for gas densities $\rho^g = 10^{-3}$ (black), 1 (blue), 3 (red) and $5\,kg/m^3$ (yellow) at $t = 1.47$ and 1.67. The grid-refinement level was $l = 3$. Reference solutions by CADYF (colored markers) [Etienne et al., 2018].
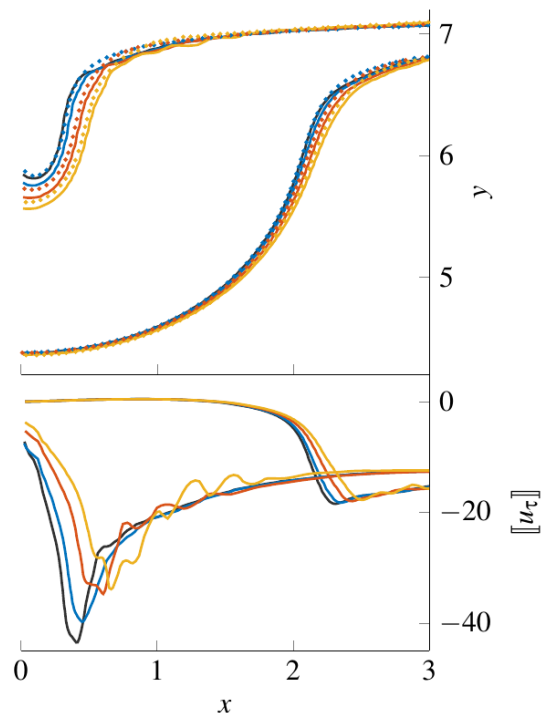
was used to achieve this. We demonstrated that this approach is able to capture contact discontinuities sharply and accurately, even at high density ratios (demonstrated up to 10^{-6}) close to the one-phase limit. After adding the effects of compressibility and viscosity, we want to use this model to study the effects of free surface instabilities in sloshing of LNG and its vapor.

References

Etienne, S., Scolan, Y.-M., and Brosset, L. (2018). Numerical study of density ratio influence on global wave shapes before impact. In *37th Int. Conf. Ocean, Offshore Arctic Eng.* Paper OMAE2018-78624.

Lafeber, W., Brosset, L., and Bogaert, H. (2012). Comparison of wave impact tests at large and full scale: Results from the Sloshel project. In *22nd Int. Symp. Offshore Polar Eng.*, volume 4, pages 285–299.

Leveque, R. J. and Li, Z. (1994). The immersed interface method for elliptic equations with discontinuous coefficients and singular sources. *SIAM J. Numer. Anal.*, 31(4):1019–1044.

Liu, X.-D., Fedkiw, R. P., and Kang, M. (2000). A boundary condition capturing method for poisson's equation on irregular domains. *J. Comput. Phys.*, 160:151–178.

Popinet, S. (2009). An accurate adaptive solver for surface-tension-driven interfacial flows. *J. Comput. Phys.*, 228(16):5838–5866.

Udaykumar, H. S., Kan, H.-C., Shyy, W., and Tran-Son-Tay, R. (1997). Multiphase dynamics in arbitrary geometries on fixed Cartesian grids. *J. Comput. Phys.*, 137(2):366–405.

Van der Plas, P. (2017). *Local Grid Refinement for Free-Surface Flow Simulations*. PhD thesis, University of Groningen.

Verstappen, R. W. C. P. and Veldman, A. E. P. (2003). Symmetry-preserving discretization of turbulent flow. *J. Comput. Phys.*, 187(1):343–368.

Wemmenhove, R., Luppes, R., Veldman, A. E. P., and Bunnik, T. (2015). Numerical simulation of hydrodynamic have loading by a compressible two-phase flow method. *Comput. Fluids*, 114:218–231.

Zinjala, H. K. and Banerjee, J. (2015). A Lagrangian-Eulerian volume-tracking with linearity-preserving interface reconstruction. *Numer. Heat Transfer, Part B*, 68:459–478.